Temperature Dependence of Hole Growth Kinetics in Aluminum−Phthalocyanine−Tetrasulfonate in Hyperquenched Glassy Water

N. C. Dang,[†] T. Reinot,*[,‡,§] M. Reppert,[†] and R. Jankowiak*[,†]

Department of Chemistry, Kansas State University, Manhattan, Kansas 66506, and Department of Chemistry, Iowa State University, Ames, Iowa 50014

Received: September 12, 2006; In Final Form: December 15, 2006

The temperature (*T*) dependence of hole growth kinetics (HGK) data that span more than four decades of burn fluence are reported for aluminum−phthalocyanine tetrasulfonate (APT) in fresh and annealed hyperquenched glassy water (HGW) for temperatures between 5 and 20 K. The highly dispersive HGK data are modeled by using the "master" equation based on the two level system (TLS) model described in 2000 by Reinot and Small [*J. Chem. Phys.* **2000**, *113*, 10207]. We have demonstrated that thermal line broadening is not enough to account for temperature-dependent HGK for temperatures greater than 10 K. To overcome the discrepancy, the hole growth model must account for thermal hole filling (THF) processes. For the first time, the "master" equation used for HGK simulations is modified to take into account both the temperature dependence of the (single site) absorption spectrum and THF processes, effectively turning off those TLS which do not participate in the hole burning process at higher temperatures. A single set of parameters, some of which were determined directly from the hole spectra, was found to provide satisfactory fits to the HGK data for APT in fresh and annealed HGW for holes burned in the 679.7−676.9 nm range from the high to low energy sides of the Q_x absorption band. Furthermore, we propose that HGK modeling at high burn fluences requires that the TLS model be further modified to take into account the existence of extrinsic multiple level systems.

1. Introduction

The phenomena of photochemical and nonphotochemical hole burning (NPHB) in the electronic absorption band of frozen Shpol'skii and glassy matrices were first reported in refs 1 and 2. It was proposed shortly thereafter that NPHB was common to glassy media and was due to interaction of the absorber with the low-frequency excitations responsible for the anomalous properties of glasses at low temperatures.[3] These low-frequency modes[4,5] were thought to be rearrangements of the glass molecules between two nearly isoenergetic configurations, typically described by double potential wells and referred to as two level systems (TLS). According to the original NPHB model,[3] hole burning occurs due to a reduced barrier between the potential minima of a TLS coupled to an absorber in its excited state. Phonon-assisted tunneling between the potential minima leads to a change in the transition frequency of the guest molecule, resulting in the "burning" of a spectral hole. The original hole burning mechanism was based on the assumption of a *static* distribution of TLS that are induced by the probe molecules (extrinsic TLS, TLS_{ext}).[3] A number of experimental findings led to the conclusion that this assumption is invalid;[6−12] this led to a refined mechanism proposed by Shu and Small.[12] These authors suggested that NPHB is the result of a hierarchy of configurational tunneling events triggered by electronic excitation of the probe. These events begin in the outer shell of the probe and involve relaxation of the faster, intrinsic TLS (TLS_{int}), which originate from the disordered nature of glassy environments and terminate in the inner shell. This outside-in chain of events results in the migration of excess free volume around the probe which leads to the final and rate-determining step: tunneling of TLS_{ext} in its excited state (TLS^{e}_{ext}).

The kinetics of NPHB, as well as of spontaneous hole filling, are highly dispersive, as has been known for two decades. The original model was based on the assumption that the dispersive kinetics are due to structural disorder and stem mainly from the distribution of tunneling rates for the TLS, referred to as the λ-distribution; this model assumed that a Gaussian shape for the λ-distribution is physically reasonable [see ref 13 and references therein]. Later, to provide better fits to HGK data, the dispersion due to photoselection caused by laser polarization (α-distribution)[14,15] and the dispersion caused by off-resonant absorption (ω-distribution)[16] were taken into account. The importance of the above distributions was analyzed in detail in ref 17, where it was demonstrated that the λ- and α-distributions were the most and least important, respectively. The resulting HGK model was further improved by incorporating the contribution from the photoproduct.[18]

In a previous study of Oxazine 720 in a glassy glycerol matrix from 1.6 to 7 K,[13] the temperature-dependent HGK were modeled by using only λ-distribution. It was concluded that the temperature dependence of the absorption rate (i.e., the change of homogeneous line width of the zero phonon line, ZPL) fully accounts for the temperature dependence of zero phonon hole (ZPH) growth kinetics, and that the tunneling relaxation rate, *R*, is independent of temperature, although the phonon-assisted tunneling rate (the rate-determining step) was shown to increase with increasing temperature. These seemingly contradictory

* Address correspondence to these authors. E-mail: ryszard@ksu.edu (R.J.) and tonu@iastate.edu (T.R.).
† Kansas State University.
‡ Iowa State University.
§ Present address: BioCrystals, LLC, 2079 Roy J. Carver, Ames, IA 50011.

10.1021/jp065958g CCC: $37.00
Published on Web 01/26/2007

results can be explained by recognizing that the thermal occupation numbers of phonons at 1.6 and 7 K are practically similar; as a result, HGK differences could easily have been buried under the noise in the study. In other words, it may be that the temperature range used was too short to observe significant temperature dependence (vide infra).

To reveal more details concerning the *T*-dependence of the hole burning rate, this paper presents results of HGK measurements in the temperature range 5−20 K for another nonphotochemical hole burning system, which has been studied extensively before,[17,19−23] aluminum phthalocyanine tetrasulfonate (APT) in fresh and annealed hyperquenched glassy water (HGW). To fully account for the temperature dependence of HGK, the following factors are considered: (1) *T*-dependence of the tunneling rate; (2) *T*-dependence of the single site absorption spectrum; and (3) thermal hole filling (THF). To study the factors considered above, a detailed calculation for the *T*-dependence of *R* is described, and we demonstrate that its effect on the *T*-dependence of the hole burning rate is negligible in the chosen temperature range. The *T*-dependence of the single site absorption spectrum was introduced by using electronic dephasing data from ref 20, and it was found that the temperature dependence of the induced absorption rate fully accounts for the temperature dependence of ZPH growth kinetics at temperatures below 10 K in agreement with the findings of ref 13. However, thermal hole filling (THF) becomes observable in APT/HGW above 10 K; it leads to additional slowdown of HGK and was taken into account by modifying the "master" equation described in ref 17. The improved model presented in this work can be used to eliminate those chromophores which do not participate in the NPHB process at higher temperatures. Note that a broader *T*-range could not be selected due to the rapid broadening of the ZPL at higher *T*.[24] The significant increase of the ZPH width requires higher burn fluences to detect the ZPH, which complicates modeling of HGK as the contributions from the phonon sideband hole (PSBH) and photoproduct have to be taken into account (see ref 18 for a detailed discussion).

2. Experimental Section

Aluminum phthalocyanine tetrasulfonate (APT) was purchased from Porphyrin Products, and nanopure water ($R \approx 18$ MΩ cm^{-1}) was used for sample preparation. A solution of APT in water with a concentration of 2×10^{-5} M was made by extensive mixing followed by filtering. The room temperature absorption spectra of APT in water were recorded, which allowed the determination of the integrated absorption cross section (σ) of the Q_x absorption band.

The apparatus used to prepare hyperquenched glassy films of water containing APT and the optical setup is described in detail in refs 19 and 20. Briefly, hyperquenched films were produced by thermospray deposition of the sample onto a polished 8 mm copper plate attached to the cold finger of a Janis ST-100 continuous flow helium cryostat. The substrate temperature was measured by a silicon diode (Lake Shore Cryogenics, DT-470) mounted directly on the back of the copper substrate on which the sample was deposited, allowing for rapid thermal equilibration and accurate temperature measurement. The temperature was monitored and stabilized by a temperature controller (Lake Shore 330 Autotuning Temperature Controller). The lowest temperature obtained was 5.0 K. The body of the cryostat was mounted in a vacuum chamber, which was continuously pumped with a turbo-molecular pump; the lowest pressure obtained was $\sim 2 \times 10^{-7}$ Torr. The thermospray was inserted into the vacuum chamber through a vacuum fitting. Thermospray inlet and outlet temperatures of 80 and 180 °C, respectively, resulted in ~2 μm diameter solution droplets. Films with thicknesses of ~10 μm were obtained on the substrate by using a reciprocating plunger pump. Films deposited at 5.0 K are referred to as *fresh* HGW. Films deposited at 5.0 K and annealed at temperature T_A for time t_A are referred to as *annealed* HGW. In this experiment $T_A = 140$ K and $t_A \approx 1$ h. Following annealing, the film was cooled to 5.0 K for spectroscopic measurements. For higher temperature measurements, the temperature controller was used to heat the sample to the desired temperature.

The optical setup consisted of an actively stabilized ring dye laser (Coherent 699-29, long-term linewidth <10 MHz, laser dye LD-688 (Exciton)) pumped by a 6 W Ar-ion laser (Coherent, Innova-90). The intensity of the laser beam was stabilized electro-optically (Brockton Electro-Optics Corp., LPC). An expander was used for the excitation beam, and laser intensity was attenuated by using a set of neutral density filters. The fluorescence was collected through a long wavelength pass filter (Omega Optical, AELP-730) and was detected with a photomultiplier tube (Hamamatsu, R2949) followed by a photon counter (Stanford Research SR400). Hole growth kinetics curves were obtained by monitoring the decrease in fluorescence intensity as a function of burn time. Multiple channel times were used in data acquisition to ensure detection of the early events in the hole-burning process.

The spectral range used for hole growth kinetics (HGK) studies was 676.9−680 nm. The low-energy side of APT's Q_x-band was chosen to avoid excitation of Q_y states, for which hole burning is significantly slower due to the competing process of $Q_y \rightarrow Q_x$ relaxation.[22] *T*-dependent HGK data were obtained at slightly different wavelengths (0.4 nm apart) in the range of 676.9−679.7 nm; it was verified that ZPH did not overlap, since overlapping holes would have interfered with HGK. Burn intensity (I_B) and burn time (t_B) were 82 nW/cm^2 and 1000 s, respectively. A burn fluence of $I_B \times t_B = 82$ μJ/cm^2 was chosen to ensure that phonon-sideband holes (PSBH) did not interfere with the ZPH peak intensity being probed.

3. Standard Hole Growth Kinetics Model

As stated in ref 17, the "master" equation based on the TLS model is given by

$$D(\Omega,t) = 1.5\int d\omega L(\Omega-\omega)G(\omega) \int d\lambda f(\lambda)\int d\alpha \sin\alpha \cos^2\alpha\, e^{-P\sigma f(\lambda)L(\omega-\omega_B)\cos^2(\alpha)t} \quad (1)$$

where $D(\Omega,t)$ is the absorption as probed at frequency Ω following a burn for time t at burn frequency ω_B ($\Omega = \omega_B$ for HGK detection). The first integral in this equation takes into account the wavelength dependence of induced absorption rate for different ω_B. ω is the frequency of the zero phonon line (ZPL), $G(\omega)$ is a Gaussian distribution of ZPL frequencies (the site-distribution function), and $L(\Omega - \omega)$ is the normalized single site absorption spectrum (vide infra). The second integral takes into account the distribution of tunneling rates which are expected to occur in a glassy matrix. λ is the tunnel parameter for the TLS_{ext}, and $f(\lambda)$ is its normalized Gaussian distribution function centered at λ_0, with a standard deviation of σ_λ. The final integral models the hole burning rate for a given TLS, taking into account the orientation-dependence of the absorption

rate for randomly oriented chromophores undergoing excitation by a linearly polarized excitation source (α-distribution). The variable α is the angle between the laser polarization and the transition dipole vectors, σ is the integrated absorption cross section ($cm^2\ s^{-1}$), and P is the photon flux (photons $cm^{-2}\ s^{-1}$). The NPHB quantum yield, $\phi(R)$, is given by $\phi(R) = R/R + \tau_{fl}^{-1}$,[13] where τ_{fl} is the excited-state lifetime of the chromophore and R is the phonon-assisted tunneling rate. Although in many systems NPHB quantum yields are very low (i.e. $\phi(R) \approx R/\tau_{fl}^{-1} \ll 1$),[25,26] the NPHB quantum yield for APT in HGW is relatively high, ~8%.[20] Therefore, the value of $\phi(R)$ in this work was calculated exactly by using $\phi(R) = R/(R + \tau_{fl}^{-1})$. The nonphotochemical hole-burning rate is determined by tunneling in the TLS_{ext}^{e}; the corresponding relaxation rate, R, is calculated by assuming that the two eigenstates of the TLS are coupled via modulation of TLS potential, which is caused by the elastic wave in the medium, i.e., a phonon. Downward processes (with creation of one phonon) should be prevalent at low temperatures; TLS−TLS interaction is neglected and electron phonon coupling is assumed to be weak ($S < 1$). For a single TLS_{ext}^{e} the phonon-assisted tunneling rate becomes:[27,28]

$$R = \left(\frac{3f^2W^2E}{16\pi\rho c^5\hbar^5}\right)(\bar{n}(E) + 1) \qquad (2)$$

where ρ is the local sample density around the probe, c is an average sound velocity, and the f parameter is related to the TLS_{ext} deformation potential.[28,29] $\bar{n}(E)$, the phonon thermal occupation number, is given by $\bar{n} = (\exp(E/kT) - 1)^{-1}$, and the tunnel splitting, E, is given by $E^2 = \Delta^2 + W^2$ (where Δ is the asymmetry parameter and W is the tunneling frequency, $W = \omega_0 \exp(-\lambda)$; see frame A of Figure 6). Because the tunneling frequency (W) depends exponentially on the tunnel parameter λ, and the tunnel splitting E may be replaced by Δ (i.e., $\Delta \gg W$), one can rewrite eq 2 as $R = \Omega_0 \exp(-2\lambda)(\bar{n}(E) + 1)$, where $\Omega_0 = 3\langle f^2\Delta\rangle\omega_0^2/16\pi\rho c^5\hbar^5$. It has been argued that $\Omega_0 \approx \omega_0$[30] and that a broad range of λ values is responsible for the distribution of relaxation rates.[15,25] Thus, a Gaussian λ-distribution can be used to describe R by using a Gaussian center value (λ_0) and standard deviation (σ_λ) which is obtained from fitting experimental HGK curves with eq 1.

$L(\Omega - \omega)$ in eq 1 is the normalized single site absorption spectrum that consists of the ZPL and phonon sideband (PSB). To model temperature-dependent hole growth kinetics, the single site absorption spectrum is expressed as[17]

$$L(\Omega - \omega) = L_{ZPL}(\Omega - \omega) \times FC + L_{PSB}(\Omega - \omega) \times (1 - FC) \qquad (3)$$

where the L_{ZPL} is the normalized Lorentzian profile of the ZPL given by

$$L_{ZPL}(\Omega - \omega) = \frac{1}{\pi}\frac{\Gamma_H(T)}{(\Omega - \omega)^2 + [\Gamma_H(T)]^2} \qquad (4)$$

FC is the Franck−Condon factor:

$$FC = \exp\{-S[2\bar{n}(\omega_m) + 1]\} \qquad (5)$$

where $\bar{n}(\omega_m) = [\exp(\hbar\omega_m/kT) - 1]^{-1}$ is the thermal occupation number for a phonon with mean phonon frequency ω_m, and S is the Huang−Rhys factor due to low-frequency phonons centered at ω_m; S is defined such that optical reorganization energy $E_{reo} = S\omega_m$. L_{PSB} is the one-phonon profile of the phonon sideband (PSB), which is approximated by a Gaussian on the low-energy side and a Lorentzian on the high-energy side.[17] $\Gamma_H(T)$ in eq 4 is given by[20,31]

$$\Gamma_H(T) = \Gamma_0 + aT^\alpha + b_1\bar{n}(\omega_1) \qquad (6)$$

where $\Gamma_0 = 1/(2\pi\tau_{fl})$ is the lifetime limited width of the ZPL. The second term, aT^α, describes dephasing due to the electron−TLS_{int} coupling. The third term is associated with dephasing due to exchange coupling with the pseudolocalized mode of frequency ω_1.[31] Amplitudes a and b_1 and the exponent α are constants and are obtained from fitting results.

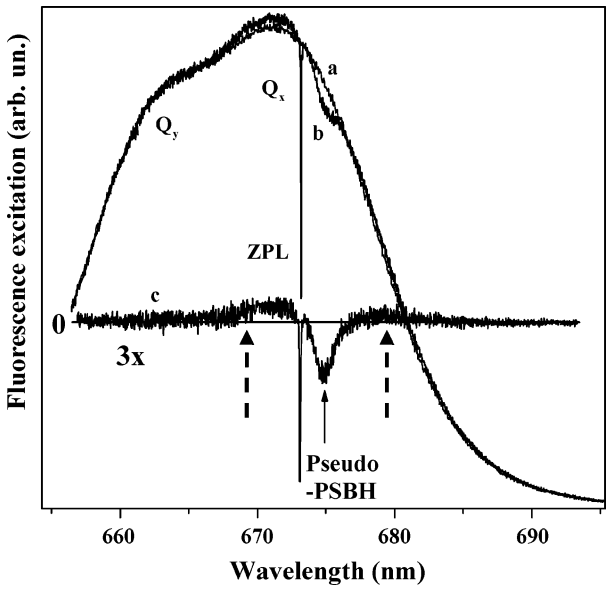

Figure 1. Preburn (a) and postburn (b) fluorescence excitation spectra of APT in fresh HGW (2×10^{-5} M) at 5 K; Q_x and Q_y mark two components of the lowest electronically excited band of APT. Curve c (curve b − curve a) shows the hole profile (×3) burned at 5 K with 15 mJ/cm^2 at 673 nm. The distances between pseudo-PSBH peak and the mean values of the blue and red photoproduct (indicated with arrows) are ~120 and ~100 cm^{-1}, respectively.

4. Results and Discussion

4.1. *T*-Dependence of Tunneling Rate. The fluorescence excitation spectrum of APT in fresh HGW is shown in Figure 1 (curve a). A hole profile of APT in fresh HGW obtained by subtracting the preburn spectrum (curve a) from the postburn spectrum (curve b) is presented as curve c in Figure 1; the hole was burned at 673.0 nm with 15 mJ/cm^2 at 5 K. For smaller burn fluences (i.e., ≤1 mJ/cm^2) the PSBH contribution was negligible and the photoproduct from the ZPH was buried within the experimental noise (data not shown). Thus, we conclude that the majority of visible photoproduct originates from the pseudo-sideband hole. The average distance of blue- and red-shifted photoproduct (see dashed arrows) from the peak of the pseudo-PSBH (solid arrow) is 120 and 100 cm^{-1}, respectively. At this burn fluence, the number of sites resulting in blue-shifted photoproduct was about 4 times the number resulting in red-shifted photoproduct.

To calculate the temperature-dependent relaxation rate R, the values of the asymmetry parameter (Δ) and the tunneling parameter (W) of the TLS_{ext}^{e} need to be estimated. Following ref 17 and references therein, we assume that the tunneling prefactor $\omega_0 \approx \Omega_0 = 7.6 \times 10^{12}$ Hz and use an average value of $\lambda_0 \approx 8.0$ for APT in HGW; these values lead to a tunneling frequency of $W \approx 0.1\ cm^{-1}$. The values of Δ_g and Δ_e, replaced

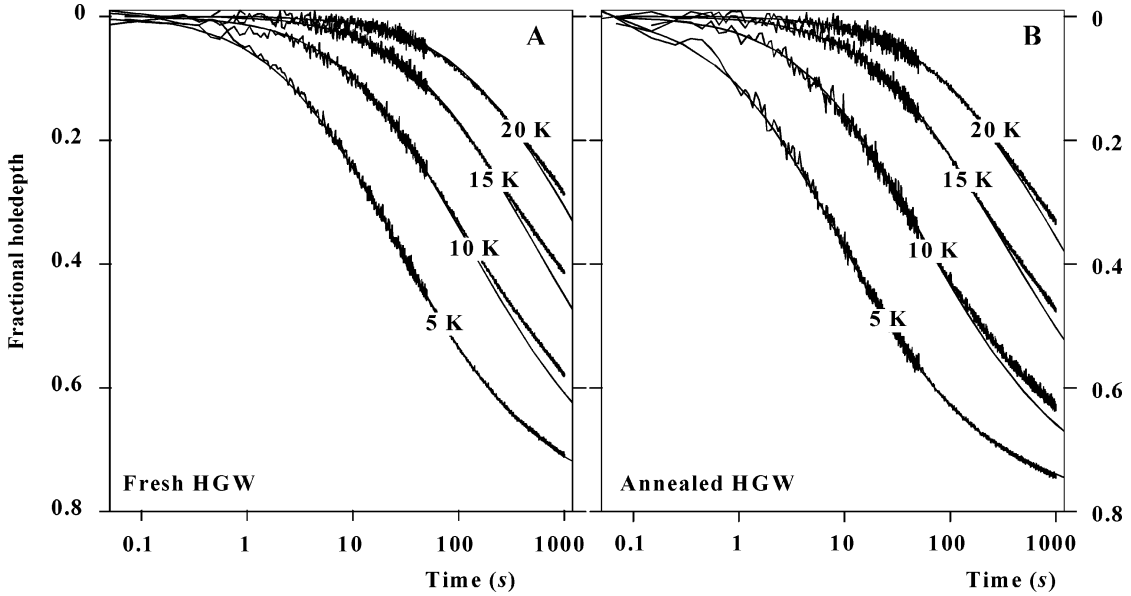

Figure 2. Normalized experimental and calculated HGK curves for APT in fresh (left) and annealed (right) HGW. Curves were obtained at different temperatures and at slightly different wavelengths (λ_B = 679.7−676.8 nm); burn intensity and time were I_B = 82 nW/cm^2 and t_B = 1000 s, respectively.

by the tunnel splitting E for the ground and excited states of TLS_{ext}, were estimated as follows. The average frequency difference between photoproduct and educt, $E_\Delta = |E_g - E_e| = |\Delta_g - \Delta_e|$, was determined from the experiment. Photoproduct from the ZPH was not observable in APT in HGW for any burn fluence used in this study; it is negligible in comparison with photoproduct originating from the PSBH (see curve c in Figure 1). In our hole burning spectra, the blue-shifted photoproduct is always more abundant. As is evident from curve c in Figure 1, even for a very shallow burn, the bulk of the photoproduct originates from the PSBH. Therefore, the value for average frequency change at hole burning was taken to be the difference between the peak of the PSBH and the average photoproduct position, resulting in a value of 120 cm^{-1} rather than 80 cm^{-1}. It was assumed that $\Delta_g/\Delta_e \approx V_g/V_e$, where V_g and V_e are barrier heights in ground and excited state TLS, respectively. The tunnel parameter used for the TLS^g_{ext} was $\lambda_{0,g}$ = 18.9,[32] and for TLS^e_{ext}, $\lambda_{0,e}$ = 8.0. Using Gamov's formula, $V = \lambda^2\hbar^2/2md^2$,[33] where d is the distance involved in tunneling and m is the mass of the tunneling entity, one can estimate that the ratio $V_g/V_e \approx \Delta_g/\Delta_e \approx 5.5$. For a TLS_{ext} with photoproduct at 120 cm^{-1} (from initial absorption frequency), the values of Δ_g and Δ_e are found to be 147 and 27 cm^{-1}, respectively. These values of asymmetry parameters result in an increase in the hole burning tunneling rate by a factor of R_{20}/R_5 = 1.17 and a decrease in the tunneling parameter of $\lambda_{0,20} - \lambda_{0,5}$ = 0.08 over the temperature range 5−20 K. This decrease in the value of λ (∼1%) is surprisingly small relative to other processes.

4.2. Thermally Induced Line Broadening and Thermal Hole Filling. Panels A and B of Figure 2 show normalized curves of HGK data (noisy curves) for APT in fresh and annealed HGW at 5.0, 10, 15, and 20 K, respectively. The smooth curves in Figure 2 are fits to the experimental data with use of eq 1 and the parameters given in Tables 1−3. It should be noted that to obtain perfect fits for the T-dependent HGK curves with eq 1, parameters λ_0, σ_λ, and S were used as free parameters. To obtain perfect fits, the T-dependent S factor was found to increase from 0.23 up to 0.55 in the temperature range of 5−20 K (data not shown). However, this increase in the value of the S factor was considered unphysical since optical reorganization energy, $S\omega_m$, does not change in the 5−20 K temperature range (see Figure 8 in ref 20). For the above reason, fitting results of T-dependent HGK data were obtained with the S factor fixed at 0.23 and 0.24 (the values found from fitting 5 K HGK data) for fresh and annealed samples, respectively, while λ_0 and σ_λ are free parameters.

It is clear from Figure 2 that hole growth kinetics in both annealed and fresh HGW slow down remarkably as temperature

TABLE 1: Parameters Used To Fit Hole Growth Kinetics Data for APT in Fresh and Annealed HGW

fwhm of site distribution function $G(\omega)$, Γ_I (cm^{-1})	356
peak phonon frequency, ω_m (cm^{-1})	37
phonon sideband (half)widths, Γ_G/Γ_L (cm^{-1})	15.5/23.5
tunnel splitting, E (cm^{-1})	27
burn time, t_B (s)	1000
fluorescence lifetime, τ_{fl} (ns) [20]	6.5
integrated absorption cross section, σ (cm^2 s^{-1})	1.75 × 10^{-2}
pre-factor of tunneling rate, Ω_o (s^{-1}) [13]	7.6 × 10^{12}

TABLE 2: Dephasing Parameters Used in Eq 6[a] for APT in Fresh and Annealed HGW

parameters	fresh HGW	annealed HGW
amplitude a (cm^{-1})	0.0011	0.00022
amplitude b_1 (cm^{-1})	7	6.9
exponent α	1.30	1.30
phonon freq ω_1 (cm^{-1})	53	50

[a] From ref 19. Due to low temperature (T < 20 K) only the lowest frequency phonon-mode (∼50 cm^{-1}) was used.

TABLE 3: Parameters Used To Fit Hole Growth Kinetics Data to Eq 1 for APT in Fresh (Left) and Annealed (Right Panel) HGW

	fresh HGW			annealed HGW		
T (K)	λ_0 (±0.03)	σ_λ (±0.03)	Γ_h (GHz)[b]	λ_0 (±0.03)	σ_λ (±0.03)	Γ_h (GHz)[b]
5	7.80	0.75	0.290	7.85	0.72	0.077
10	7.90	0.78	0.786	8.00	0.75	0.310
15	8.05	0.80	2.450	8.03	0.80	1.970
20	8.10	0.80	6.390	8.10	0.81	6.180

[a] Holes were burned with a burn time (t_B) of 1000 s and burn intensity (I_B) of 82 nW/cm^2. The Huang Rhys factor, S, was found from fits to 5 K data to be 0.23 for fresh HGW and 0.24 for annealed HGW. [b] ±1−3%.

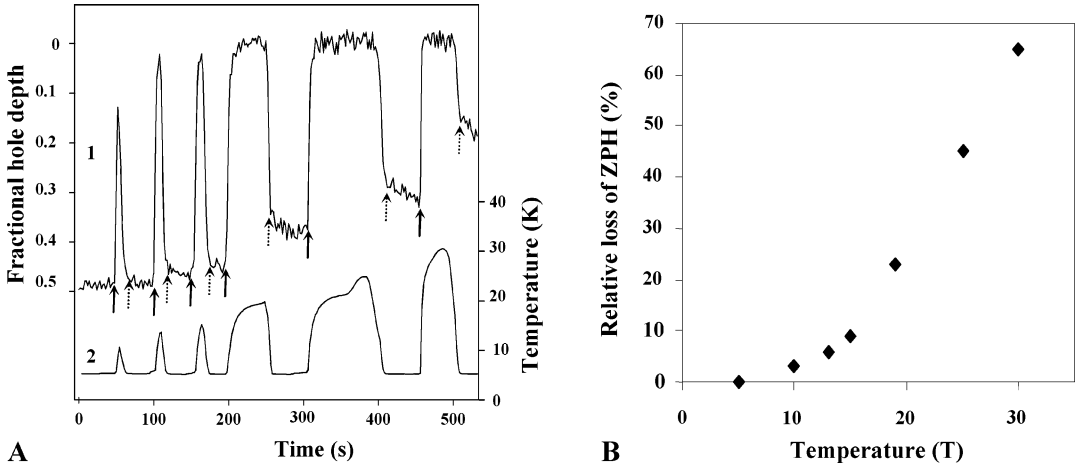

Figure 3. A ZPH with fractional depth of 0.48 was burned into APT in fresh HGW at 680.2 nm with $I_B = 70$ nW/cm^2, $t_B = 60$ s, and at $T = 5$ K. Fractional hole depth (curve 1) is recorded as a function of time as the temperature is varied from 5 to 30 K; curve 2 shows sample temperature as a function of time. Vertical arrows mark fractional hole depths before (solid arrows) and after (dotted arrows) thermal cycles; these data were used to calculate relative thermal hole filling (see text for details).

increases. The broadening of the zero phonon line and the increasing contribution from the PSB hole are the primary causes of the HGK slowdown. This is evidenced by the observation that, if HGK data for fresh HGW are fitted with use of eq 1, while neglecting the temperature dependence of the absorption profile $L(\omega - \omega_B)$, the value of λ_0 was found to be 8.1 at 5 K and 10.2 at 20 K, an increase of ~26%. A similar increase in the value of λ_0 was found for annealed HGW. This increase is considered to be physically unreasonable. However, if HGK data are fitted with eq 1 (including T-dependence of the absorption profile), the value of λ_0 increases from 7.80 at 5 K to 8.10(±0.03) at 20 K for fresh HGW and from 7.85 at 5 K to 8.10(±0.03) at 20 K for annealed HGW, an increase of roughly 3% between 5 and 20 K. The increase of λ_0 by a factor of 0.03 would lead to $R_{20}/R_5 = 1.8$, which is a factor of ~1.5 larger than that found in section 4.1. This indicates that the temperature dependence of the absorption profile cannot fully account for the T-dependence of HGK. It is clear, then, that there must be an additional contribution to the temperature dependence as evidenced by the increasing discrepancy between calculations and experimental results in Figure 2.

Fitting HGK curves as a function of temperature resulted in "poor" fits with greater discrepancy at longer hole burning times. The faster burning rates of HGK found from fitting results are most probably caused by the neglect of a fitting term for photoproduct and, consequently, all interference effects arising from photoproduct, i.e., spontaneous hole filling (SHF) in the ground state, light induced hole filling (LIHF), and thermal hole filling (THF). THF starts to contribute to HGK in APT in HGW when the temperature approaches 10 K as is clearly illustrated in Figure 3. In this figure, first, a ZPH with fractional depth of 0.48 was burned for 60 s in APT in fresh HGW at 680.2 nm with a burn intensity of 70 nW/cm^2 ($T = 5$ K). The laser was kept at burn frequency with the laser intensity reduced to 6 nW/cm^2; the fluorescence signal was then detected as a function of time (curve 1), while the sample temperature was cycled as is shown in Figure 3 (curve 2). This allowed measurement of the ZPH depth at 5 K before and after each thermal cycle. A relative loss of ZPH depth can be calculated as the percentage difference between the fractional hole depths before and after each thermal cycle (as indicated in the figure by solid and dotted arrows, respectively), which is 2%, 6%, 8%, 24%, 45%, and 65%, after thermal cycling to 10, 13, 15, 19, 25, and 30 K, respectively. The effect is more clearly illustrated in frame B of Figure 3, where relative loss of ZPH is plotted as a function of excursion temperature. Note from Figure 3A that ZPH depth starts to recover after each thermal cycle as a fraction of the thermally filled sites are quickly burned away. It should also be noted that the HGK of partially filled holes are very fast in the beginning and slow down remarkably as initial hole depth is approached. This is easily seen from the figure at temperature excursions above 20 and 25 K. In other words, HGK are different when compared to those of "unaffected" sites burned at 5 K in a "virgin" sample (data not shown). This is most likely caused by different distributions of hole burning sites.

TABLE 4: Parameters Used To Fit HGK Data of APT in Fresh and Annealed HGW (Figure 4) to Eq 12[a]

	fresh HGW			annealed HGW		
T (K)	λ_0 (±0.03)	σ_λ (±0.03)	$1 - p(T)$	λ_0 (±0.03)	σ_λ (±0.03)	$1 - p(T)$
5	8.25	0.85	0.00	8.15	0.75	0.00
7	8.25	0.88	0.01	8.15	0.80	0.01
9	8.25	0.90	0.02	8.15	0.87	0.02
11	8.25	0.95	0.04	8.15	0.91	0.04
13	8.25	1.00	0.07	8.15	0.98	0.07
15	8.25	1.05	0.10	8.15	1.05	0.10
18	8.25	1.07	0.17	8.15	1.07	0.17
20	8.25	1.10	0.25	8.15	1.10	0.25

[a] Holes were burned with a burn time (t_B) of 1000 s and burn intensity (I_B) of 82 nW/cm^2.

The differences observed between the experimental and calculated HGK curves at temperatures >10 K are most likely due to interference between HB and THF; hence, the "master" equation must be modified to account for the THF processes (vide infra). THF is a thermally activated process in the ground state, which returns hole burned sites with low barrier heights back to their origin state. If it happens at the time HGK is detected, then the detected HGK are slower and the resulting ZPH is shallower. Therefore, due to competition between hole burning and THF processes at high temperature, a portion of the TLS contributing to HGK *do not burn persistently*. A simple modification of eq 1 accounts for THF processes in cases of low burn fluences (i.e., when PSBH and product band are not observed in the absorption spectrum, vide infra).

To account for THF, first it should be noted that the barrier heights and tunneling rates of TLS_{ext} are related, $V \propto \lambda^2$ (see section 4.1). Sites with faster kinetics (smaller λ) also have lower barriers, allowing separation of the λ-distribution (as well as

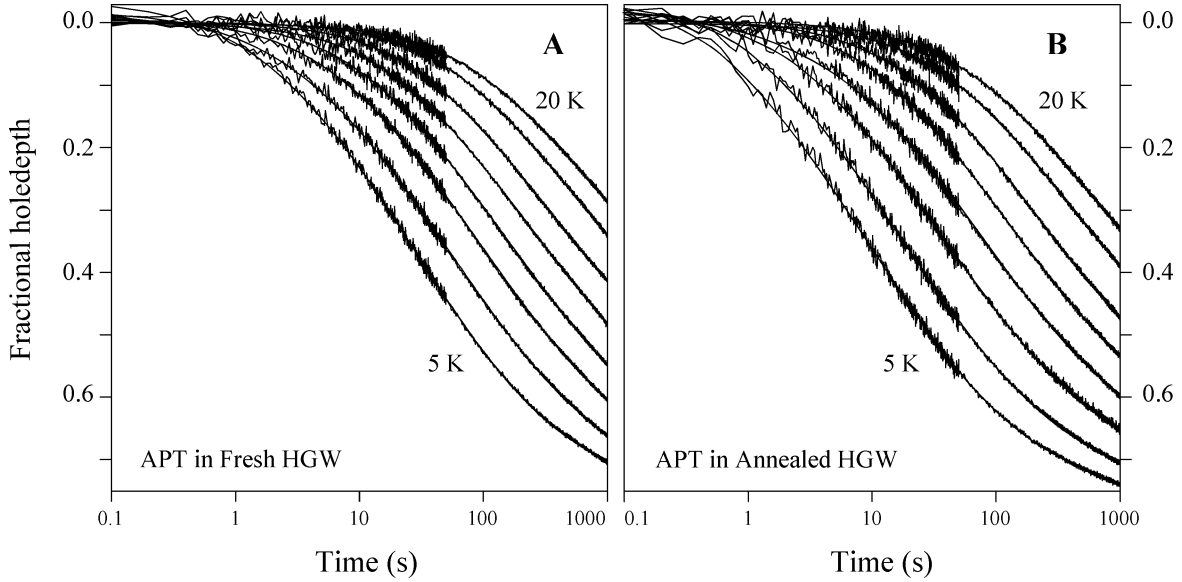

Figure 4. Normalized experimental (noisy curves) and calculated HGK data (smooth curves) for APT in fresh (frame A) and annealed (frame B) HGW. Curves from bottom to top were obtained at different temperatures: 5, 7, 9, 11, 13, 15, 18, and 20 K, respectively. Burn intensity and burning time were $I_B = 82$ nW/cm^2 and $t_B = 1000$ s, respectively.

eq 1) into two parts accounting for fast and slow relaxation processes. We define a temperature-dependent step-function:

$$H(T) = \left(1 + \exp\left[\frac{\lambda_{step}(T) - \lambda}{c}\right]\right)^{-1} \quad (7)$$

where λ_{step} is a function of temperature defined so that $H(T) = 0$ for $\lambda < \lambda_{step}$ and $H(T) = 1$ for $\lambda > \lambda_{step}$. c provides a finite width to the step. A percentile, given by $p(T) = \int d\lambda f(\lambda)H(T)$, represents the fraction of sites that are persistently burned at a given temperature. Similarly, $p(T)$ gives the fraction of photon flux that burns a persistent hole. Thus eq 1 can be rewritten as

$$D(\Omega,T,t) = D_{slow}(\Omega,T,t) + D_{fast}(\Omega,T,t) \quad (8)$$

where $D_{slow}(\Omega,T,t)$ and $D_{fast}(\Omega,T,t)$ are given by eqs 9 and 10:

$$D_{slow}(\Omega,T,t) = 1.5\int d\omega L(\Omega - \omega)G(\omega)\int d\lambda f(\lambda)H(T) \int d\alpha \sin\alpha \cos^2\alpha\, e^{-Pp(T)\sigma\phi(\lambda)L(\omega-\omega_B)\cos^2(\alpha)t} \quad (9)$$

$$D_{fast}(\Omega,T,t) = 1.5\int d\omega L(\Omega - \omega)G(\omega)\int d\lambda f(\lambda)(1 - H(T)) \int d\alpha \sin\alpha \cos^2\alpha\, e^{-P(1-p(T))\sigma f(\lambda)L(\omega-\omega_B)\cos^2(\alpha)t} \quad (10)$$

Equation 9 describes the absorption spectrum of sites which are burned persistently, and eq 10 describes the absorption spectrum of sites which are burned but are rapidly refilled by thermally induced hole filling processes. The NPHB quantum yield, $\phi(R) = \phi(\lambda)$, is given for both eqs 9 and 10 by the following: $\phi(\lambda) = (H(T)\Omega_0 \exp(-2\lambda))/(\Omega_0 \exp(-2\lambda) + \tau^{-1})$. Equation 10 can be simplified because $\phi(\lambda) = 0$ for $\lambda < \lambda_{step}$ (i.e., the exponent in eq 10 is equal to 1) and the coefficient $[1 - H(T)] = 0$ for $\lambda > \lambda_{step}$. As a result, $D_{fast}(\Omega,T,t)$ can be written as

$$D_{fast}(\Omega,T,t) = \int d\omega L(\Omega - \omega)G(\omega)[1 - p(T)] \quad (11)$$

and represents a temperature-dependent, constant in time (i.e., "nonburning") background. Thus, taking eqs 8 to 11 into account, the temperature-dependent HGK can be described as

$$D(\Omega,T,t) = \int d\omega L(\Omega - \omega)G(\omega) \times (1 - p(T) + 1.5\int d\lambda f(\lambda)H(T)\int d\alpha \sin\alpha \cos^2\alpha\, e^{-Pp(T)\sigma f(\lambda)L(\omega-\omega_B)\cos^2(\alpha)t}) \quad (12)$$

This equation takes into account both the T-dependent absorption profile and static thermal hole filling by using the function $H(T)$ to "switch off", as a function of temperature, the TLS that do not participate in hole burning.

Equation 12 provides perfect fits (smooth curves) for HGK data (noisy curves) for APT in fresh HGW (frame A) and annealed HGW (frame B) as illustrated in Figure 4. HGK data were measured at temperatures 5, 7, 9, 11, 13, 15, 18, and 20 K in the range 676.9−679.7 nm. Holes were burned 0.4 nm apart, starting at 679.7 nm. As is expected, the value of λ_0 and the Huang−Rhys factor S were found to be constant and physically reasonable for both samples in the 5−20 K temperature range. The constant values of λ_0 and S were 8.25 ± 0.02 and 0.23 ± 0.01, respectively, for APT in fresh HGW. Similarly, values of $\lambda_0 = 8.15 \pm 0.02$ and $S = 0.24 \pm 0.01$ were found for APT in annealed HGW. Interestingly, σ_l increases from 0.85 to 1.10 for fresh HGW and from 0.75 to 1.10 for annealed HGW when the temperature is increased from 5 to 20 K. The increase is apparent and most likely due to a simplified treatment of the photoproduct in eq 12. Another factor is that the TLS model gradually loses its applicability with increasing temperature (vide infra).

It is known that hole burning at high temperatures requires high burn fluence, which leads to interference of the ZPH with photoproduct and the phonon sideband hole (PSBH). This interference complicates modeling of spectral hole burning. There are two observations that demonstrate the limited applicability of the TLS model. First, it has been observed that very sharp and intense blue-shifted photoproduct and deep PSBH (~85%) at sufficiently high burn fluences become major hole shape determining factors and lead to the breakdown of the TLS model.[23,34] The change of shape and position of photoproduct has been explained by using multiple level systems

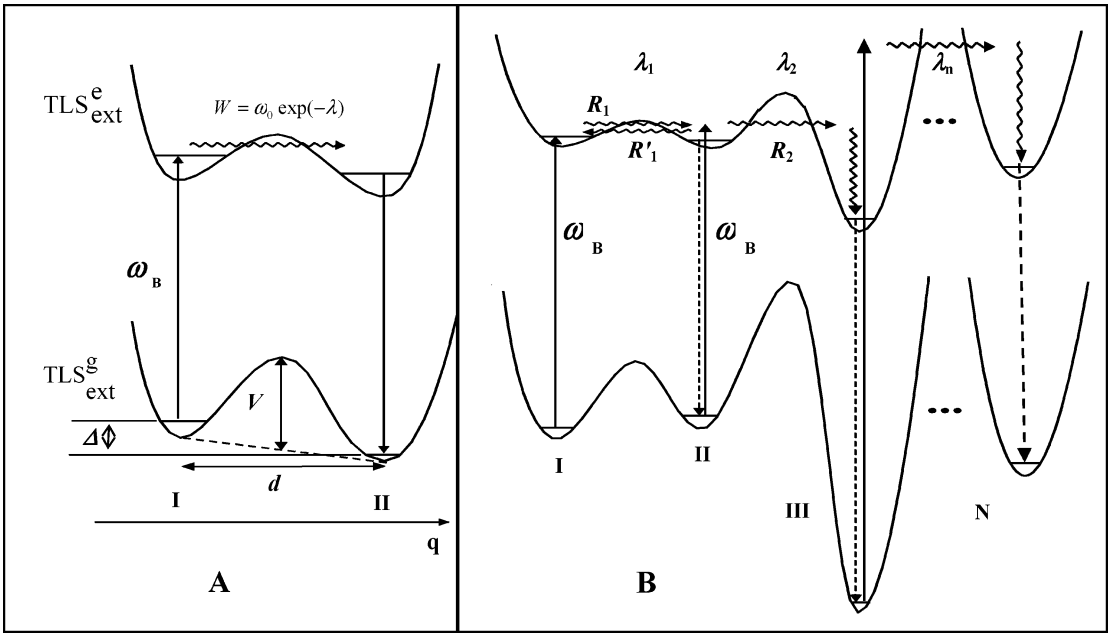

Figure 5. Frame A defines the TLS parameters. Frame B shows a schematic of MLS model for NPHB. In frame A, indices *e* and *g* indicate the chromophore in its excited and ground state. ω_B is the burn frequency, *W* is the tunneling frequency, Δ is asymmetry parameter, *d* is the displacement between the two potential energy minima, and *V* denotes TLS barrier height. In frame B, I, II, III, and N denote different chromophore−host configurations where I is the preburn configuration and II, ..., N are postburn configurations. Each pre- and postburn configuration pair ($i = 1, 2, ..., n$) is characterized by different tunneling parameters (W, Δ, V, d, R, and λ) forming different distributions.

(MLS),[23,34] which is shown in the right frame of Figure 5. Briefly, burning of configuration I with rate constant k_1 leads to anti-hole (photoproduct) configuration II, whose ZPL is red-shifted relative to ω_B. Following relaxation to the ground state, configuration II can absorb ω_B photons via its phonon sideband and revert to configuration I with rate constant k_2. Configuration I can then be re-excited and converted to configuration II. This process could be repeated many times. However, configuration II can also be converted to configuration III (with rate constant k_3), which is blue-shifted relative to ω_B. With $k_3 \ll k_2$ and the II $\rightarrow$ III conversion being essentially irreversible, multiple excitations eventually lead to an anti-hole that is entirely blue-shifted relative to ω_B. Note that configuration III in frame B can absorb at ω_B via phonon sideband transitions.

Second, due to configurational changes of TLS at high temperatures, those TLS_{ext} which participate in hole burning at low temperatures may not participate persistently in hole burning at high temperatures (i.e., at $T > 20$ K). As a consequence, a single distribution of TLS_{ext} cannot account for high-temperature hole burning. For example, to observe a ZPH with a fractional hole depth of 0.7 (e.g., at 5 K) it is required to burn all resonant TLS_{ext}. After thermal cycling from 5 to 50 K such a ZPH fills completely (data not shown). However, even at 78 K, a ZPH with a fractional hole depth of 0.45 can be observed in APT in HGW, and hole burning is possible up to 125 K.[19] It appears, then, that different distributions of TLS_{ext} are responsible for the observed hole burning at low and high temperatures, respectively. The possibility of burning deep holes above 50 K requires, therefore, more than one TLS_{ext} per single chromophore, i.e., one needs to incorporate a multiple level system (MLS) model for hole burning at high temperature.

5. Concluding Remarks

The temperature dependence of hole growth kinetics in aluminum phthalocyanine tetrasulfonate in hyperquenched glassy water was studied in the temperature range from 5 to 20 K. This study shows that the temperature dependence of the hole burning rate becomes significantly less important when the temperature induced absorption rate is taken into account for temperatures below 10 K. However, as the temperature approaches 10 K and above, it is found that the *T*-dependence of the absorption rate is not enough to account for the *T*-dependence of the hole growth rate at longer burning times. We argue that the additional slowdown of the hole growth rate as temperature increases is associated with THF, a process that prevents faster burning chromophores from contributing to the persistent spectral hole. THF processes become significant at ~10 K in APT in hyperquenched water glass and they lead to the breakdown of the two level system model for nonphotochemical hole burning at $T > 10$ K. We account for the THF process by modifying the "master" equation so as to eliminate those chromophores in the TLS model that do not participate in the persistent nonphotochemical hole burning process at temperatures higher than 10 K.

It should be emphasized that eq 12 (and the model for single distribution of TLS_{ext}) is not suitable to model HGK data that are burned at high temperature (i.e., at $T > 20$ K) with high burn fluences. For the reasons discussed above, hole burning models at high temperatures with high burn fluences must simultaneously take into account both photoproduct and the existence of MLS. This improvement, however, is beyond the scope of this paper and will be published separately. Readers who are interested in a theoretical hole burning model that takes photoproduct into account are referred to ref 18 for a detailed discussion. To account for the existence of MLS, we propose a new hole burning model where multiple level systems can be incorporated into eq 12 by introducing different λ-distributions (λ_i) with $i = 1, ..., n$. (Since multiple potential wells would couple with the same chromophore, different pairs of TLS could be characterized by different tunneling coordinates leading to distinctly different λ-distributions.) Equation 12 can then be rewritten as follows:

$$D(\Omega,T,t) = \int d\omega L(\Omega - \omega)G(\omega) \times \prod_i \left(1 - p_i(T) + 1.5\int d\lambda_i f(\lambda_i)H_i(T) \int d\alpha \sin\alpha \cos^2\alpha\, e^{-Pp_i(T)\sigma\phi(\lambda_i)L(\omega-\omega_B)\cos^2(\alpha)t}\right) \quad (13)$$

where index i labels normalized Gaussian distribution functions $f(\lambda_i)$, with different center values $\lambda_{0,i}$ and standard deviations $\sigma_{0,i}$. We emphasize that this concept is not the same as one with a very broad or non-Gaussian λ distribution. In the TLS model, a persistent hole saturates when competing hole growth and filling rates become equal due to SHF, THF, or LIHF processes. In contrast, in a three level system model such a balance is expected at higher fluences, and in a MLS model such a balance may not occur at all. This prediction is consistent with our experimental data obtained for APT in HGW, in which we were unable to saturate the hole growth for fluences ranging from nJ/cm^2 up to kJ/cm^2.[23,34] Thus, the TLS model works well at low temperatures and at moderate and low burn intensities. Under these conditions, the burn fluence, $f = I_B \times t_B$, is a good characteristic for hole growth (i.e., two holes are identical if burned with the same fluence but with different t_B and I_B). However, at temperatures higher than ~20 K, due to multiple level systems and competition between the growth and filling processes, fluence alone is not a good parameter to fit HGK since the hole growth process primarily depends on I_B while the filling process depends primarily on t_B.

Acknowledgment. In memory of Professor Gerald J. Small. We acknowledge Dr. John M. Hayes and Prof. Gerald J. Small for useful discussions during the early stage of this project. This research was supported by the Solid State Chemistry and Polymers Program of NSF under Grant No. DMR-9908714.

References and Notes

(1) Gorokhovskii, A.; Kaarli, R.; Rebane, L. A. *JETP Lett.* **1974**, *20*, 216.
(2) Kharlamov, B. M.; Personov, R. I.; Bykovskaya, L. A. *Opt. Commun.* **1974**, *12*, 191.
(3) Hayes, J. M.; Small, G. J. *Chem. Phys.* **1978**, *27*, 151.
(4) Anderson, P. W.; Halperin, B. I.; Varma, C. M. *Philos. Mag.* **1972**, *25*, 1.
(5) Phillips, W. A. *J. Low Temp. Phys.* **1972**, *7*, 351.
(6) Bogner, V.; Schwarz, R. *Phys. Rev. B* **1981**, *24*, 2846.
(7) Jankowiak, R.; Bässler, H. *J. Mol. Electron.* **1985**, *1*, 73.
(8) Childs, F.; Francis, A. H. *J. Phys. Chem.* **1985**, *89*, 466.
(9) Kohler, W.; Friedrich, J.; Fisher, R.; Scheer, H. *J. Chem. Phys.* **1988**, *89*, 871.
(10) Johnson, S. G.; Small, G. J. *Chem. Phys. Lett.* 1989,*155*, 371.
(11) Gillie, J. K.; Small, G. J.; Golbeck, J. H. *J. Phys. Chem.* **1989**, *93*, 1620.
(12) Shu, L.; Small, G. J. *Chem. Phys.* **1990**, *141*, 447.
(13) Kenney, M. J.; Jankowiak, R.; Small, G. J. *Chem. Phys.* **1990**, *146*, 47.
(14) Köhler, W.; Breinl, W.; Friedrich, J. *J. Phys. Chem.* **1985**, *89*, 2473.
(15) Elschner, A.; Bässler, H. *Chem. Phys.* **1988**, *123*, 305.
(16) Köhler, W.; Friedrich, J. *Chem. Phys. Lett.* **1987**, *134*, 200.
(17) Reinot, T.; Small, G. J. *J. Chem. Phys.* **2000**, *113*, 10207.
(18) Reinot, T.; Dang, N. C.; Small, G. J. *J. Chem. Phys.* **2003**, *119*, 10404.
(19) Kim, W.-H.; Reinot, T.; Hayes, J. M.; Small, G. J. *J. Phys. Chem.* **1995**, *99*, 7300.
(20) Reinot, T.; Kim, W.-H.; Hayes, J. M.; Small, G. J. *J. Chem. Phys.* **1996**, *104*, 793.
(21) Reinot, T.; Hayes, J. M.; Small, G. J. *J. Chem. Phys.* **1997**, *106*, 457.
(22) Reinot, T.; Hayes, J. M.; Small, G. J.; Zerner, M. C. *Chem. Phys. Lett.* **1999**, *299*, 410.
(23) Reinot, T.; Small, G. J. *J. Chem. Phys.* **2001**, *114*, 9105.
(24) Hayes, J. M.; Lyle, P. A.; Small, G. J. *J. Phys. Chem.* **1994**, *98*, 7337.
(25) Jankowiak, R.; Small, G. J. *Science* **1987**, *273*, 628.
(26) Jankowiak, R.; Shu, L.; Kenny, M. J.; Small, G. J. *J. Lumin.* **1987**, *36*, 293.
(27) Jäckle, J.; Piche, L.; Arnold, W.; Hunklinger, S. *J. Non-Cryst. Solids* **1976**, *20*, 365.
(28) Jankowiak, R.; Hayes, J. M.; Small, G. J. *Topics in Current Physics, Persistent Spectral Hole Burning: Science and Applications*; Moener, W. E., Ed.; Springer: Berlin, Germany, 1987; p 153.
(29) Phillips, W. A., Ed. *Amorphous Solid-Low Temperature Properties*; Springer: Berlin, Germany, 1981.
(30) Reichert, P.; Schilling, R. *Phys. Rev. B* **1985**, *32*, 5731.
(31) Silbey, R.; Kassner, K. *J. Lumin.* **1987**, *36*, 283.
(32) Reinot, T.; Hayes, J. M.; Small, G. J. *J. Chem. Phys.* **1999**, *110*, 4820.
(33) Davydow, A. S. *Quantum Mechanics*; VEB Deutsches, Verlag der Wissenschaften: Berlin, Germany, 1970.
(34) Reinot, T.; Hayes, J. M.; Small, G. J. *J. Phys. Chem. B* **2001**, *105*, 5083.